

Subthreshold Photoionization Spectra of CH₃I Perturbed by SF₆

C. M. Evans^{a,b}, R. Reininger^a and G. L. Findley^a

^aDepartment of Chemistry, Northeast Louisiana University, Monroe, LA 71209

^bCenter for Advanced Microstructures and Devices (CAMD) and
Department of Chemistry, Louisiana State University, Baton Rouge, LA 70803

We present pressure-dependent and temperature-dependent subthreshold photoionization spectra of pure CH₃I (up to 200 mbar) and CH₃I doped into SF₆ (up to 1 bar). At the high pressures studied, no temperature effect is observed for the subthreshold structure, thus ruling out vibrational autoionization of CH₃I as an ionization mechanism. Moreover, analysis of photocurrent intensities as a function of CH₃I number density (pure CH₃I) and SF₆ number density (CH₃I doped into SF₆) shows a quadratic dependence in the former case and a linear dependence in the latter case. This is discussed in terms of dopant (D)/perturber (P) interactions involving the excited state processes $D^* + P \rightarrow D^+ + P^-$ and $D^* + P \rightarrow [DP]^+ + e^-$, where D^* is a discrete Rydberg state of the dopant (CH₃I). From the density dependence of the subthreshold structure of CH₃I/SF₆, the electron scattering length in SF₆ is determined and compared to a value recently obtained from autoionizing states in the same system.

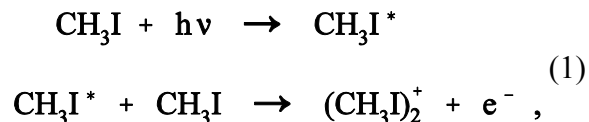
1. INTRODUCTION

Methyl iodide (CH₃I) has served as a convenient probe in studies of high-*n* Rydberg dopant-perturber interactions [1-7]. Dopant/perturber systems have included CH₃I/rare gases [1-4], CH₃I/H₂ [4], CH₃I/alkanes [5], CH₃I/CO₂ [6] and CH₃I/N₂ [7]. Both photoabsorption and photoionization spectra have been measured, and perturber pressure effects have been analyzed for discrete and autoionizing dopant Rydberg states [1-7], as well as for subthreshold photoionization structure [3,6,7].

Photoionization spectra of CH₃I [8-11] and of CH₃I doped into Xe [3], CO₂ [6] and N₂ [7] exhibit rich subthreshold structure beginning 0.17 eV before the ionization limit $I_1 \equiv I(^2E_{3/2})$. From the observed energy spacing and linear shift (as a function of perturber number density) of these peaks, the subthreshold structure has been identified as arising from high-*n* Rydberg states of CH₃I, which permitted the evaluation of electron scattering lengths in highly

absorbing perturber media [3,6,7].

Ivanov and Vilesov [9] discussed vibrational autoionization as a possible source of the subthreshold signal in pure CH₃I at pressures below 10⁻³ mbar. At higher pressures, however, they proposed [8,9] that subthreshold photoionization results from the Hornbeck-Molnar [12] process, namely,



as observed in the rare gases. (Here, $h\nu$ is the photoexcitation energy and CH_3I^* represents a Rydberg state.)

From a study of the temperature dependence of the relative peak heights of the subthreshold structure in pure CH₃I, Meyer, Asaf and Reininger [11] were able to demonstrate that the ionization mechanism is vibrational autoionization at pressures up to 15 x 10⁻³ mbar. This pressure is one order of magnitude greater than the pressure limit cited by Ivanov and

Vilesov [9], after which these authors [9] claimed to have observed a quadratic dependence of photocurrent signal on CH₃I pressure (in accord with process (1), above).

In a recent work [13], we measured the linear shift of autoionizing states of CH₃I perturbed by SF₆, in the region $I_1 < h\nu < I_2$ [$\equiv I(^2E_{1/2})$], as a function of SF₆ number density in order to extract the electron scattering length in SF₆. In the present paper, we report both pressure-dependent and temperature-dependent subthreshold photoionization spectra of pure CH₃I (up to 200 mbar) and CH₃I doped into SF₆ (up to 1 bar). Our results confirm a quadratic dependence of photocurrent signal upon CH₃I pressure in the subthreshold region of pure CH₃I at high pressure, with no temperature dependence indicative of vibrational autoionization. For CH₃I/SF₆, we observe a linear dependence of photocurrent signal upon SF₆ pressure in the subthreshold region, again with no temperature effect. This latter result suggests a possible analog of process (1), namely



Finally, we have used the subthreshold structure of CH₃I/SF₆ photoionization to extract the electron scattering length in SF₆ and find that this value accords with our previously reported result [13].

2. EXPERIMENT

Photoionization and photoabsorption spectra were measured with monochromatized synchrotron radiation having a resolution of 0.13 nm (200 μ slits), or ~ 10 meV in the spectral range of interest. Two different cells were used: Cell 1 [14] is equipped with entrance and exit LiF windows and a pair of parallel-plate electrodes (stainless steel, 3.0 mm spacing) oriented perpendicular to the windows, thus permitting the simultaneous recording of transmission and photoionization spectra. The

light path inside the cell is 1.0 cm. Cell 2 [15] is equipped with an entrance LiF window coated with a thin (7 nm) layer of gold to act as an electrode. A second electrode (stainless steel) is placed parallel to the window with a spacing of 1.05 mm. The bodies of both cells are fabricated from copper and are capable of withstanding up to 100 bar. Each cell was connected to a cryostat and heater system allowing the temperature to be controlled to within 1 K [14]. The applied electric field was 100 V, with the negative electrode being the LiF window in cell 2. (The reported spectra are current saturated, which was verified by measuring selected spectra at different electric field strengths.) Photocurrents within the cell were of the order of 10^{-10} A.

The intensity of the synchrotron radiation exiting the monochromator was monitored by measuring the photoemission current from a metallic grid intercepting the beam prior to the experimental cell. All photoionization spectra are normalized to this current. Transmission spectra (which are reported as absorption = 1 - transmission) were normalized both to the incident light intensity and to the empty cell transmission.

CH₃I (Aldrich Chemical Company, 99%) and SF₆ (Matheson Gas Products, 99.996%) were used without further purification. The gas handling system has been described previously, as well as the procedures employed to ensure a homogeneous mixing of CH₃I with SF₆ [5].

3. RESULTS AND DISCUSSION

Representative subthreshold photoionization spectra for pure CH₃I at varying CH₃I pressures (number densities) are presented in Fig. 1 in comparison to the low-pressure photoabsorption spectrum of CH₃I. Similar spectra are shown in Fig. 2 for CH₃I doped into varying number densities of SF₆. (All of the photoionization spectra presented are normalized to unity at the same spectral feature above the CH₃I $^2E_{3/2}$ threshold.) In both systems, one observes

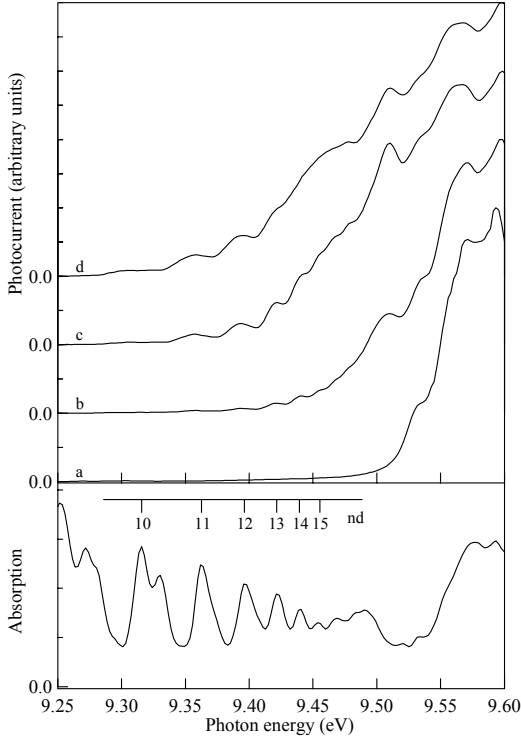


Fig. 1. Subthreshold photoionization spectra of CH_3I at 299K. Absorption of pure CH_3I (Cell 1, 200 μ slits): 0.1 mbar. Photoionization (Cell 2, 200 μ slits) at varying CH_3I number densities (10^{19} cm^{-3}): a, 0.0024; b, 0.025; c, 0.12; d, 0.49. Each photoionization spectrum is normalized to unity at the same spectral feature above the ${}^2E_{3/2}$ ionization threshold.

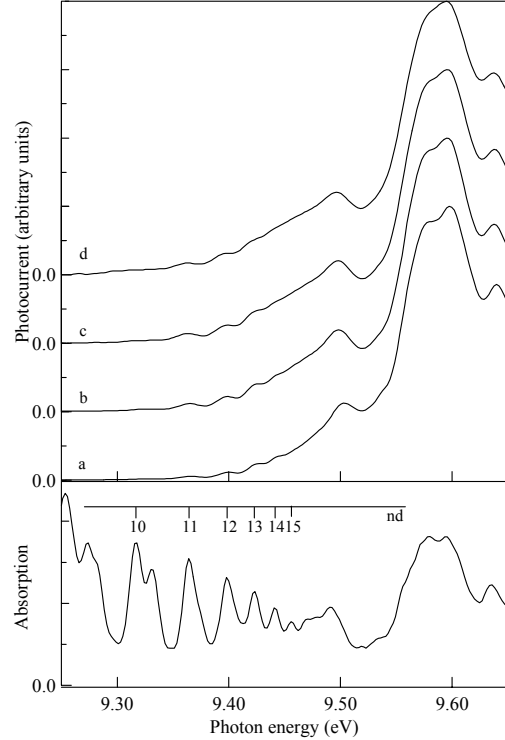


Fig. 2. Subthreshold photoionization spectra of $\text{CH}_3\text{I}/\text{SF}_6$ at 298K. Absorption of pure CH_3I (Cell 1, 200 μ slits): 0.1 mbar. Photoionization (Cell 1, 400 μ slits) of 0.1 mbar CH_3I in varying SF_6 number densities (10^{19} cm^{-3}): a, 0.13; b, 0.73; c, 1.22; d, 1.82. Each photoionization spectrum is normalized to unity at the same spectral feature above the ${}^2E_{3/2}$ ionization threshold.

subthreshold photoionization structure that correlates with nd Rydberg states of CH_3I converging on the ${}^2E_{3/2}$ ionization limit. In order to ascertain whether or not the high-pressure subthreshold structure arises from the vibrational autoionization mechanism demonstrated by Meyer, Asaf and Reininger [11] in low-pressure pure CH_3I (where the photocurrent signals are at least two orders of magnitude less than those reported here), we measured photoionization spectra for one sample pressure at different temperatures. These results are shown in Fig. 3 for pure CH_3I , and in Fig. 4 for $\text{CH}_3\text{I}/\text{SF}_6$. Clearly, there is no temperature effect on the relative intensities of the subthreshold peaks, thus ruling out vibrational autoionization as the ionization mechanism in the high-pressure case.

We extracted peak areas (by gaussian fits to the photoionization spectra) for the density-dependent subthreshold structure of pure CH_3I and CH_3I doped into SF_6 . These data are collected in Table I (CH_3I) and Table II ($\text{CH}_3\text{I}/\text{SF}_6$), and plotted in Fig. 5 (CH_3I) and Fig. 6 ($\text{CH}_3\text{I}/\text{SF}_6$). Figure 5 clearly shows a quadratic dependence on CH_3I number density, as claimed by Ivanov and Vilesov [9], in accord with process (1). Equally clearly, Fig. 6 exhibits a linear dependence on SF_6 number density, which accords with the suggested process (2). (An analysis of peak heights as opposed to peak areas gives rise to plots identical in shape to those shown here.)

Since the subthreshold photoionization structure of Figs. 1 and 2 is superimposed upon a rising exponential background, as discussed

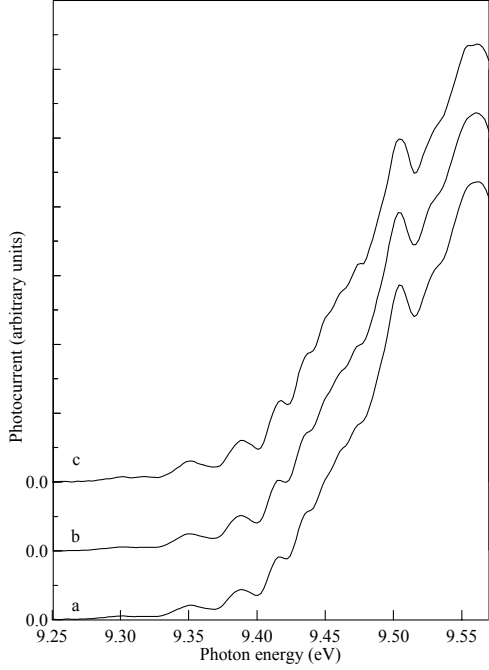
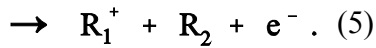
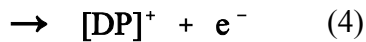


Fig. 3. Temperature dependence of subthreshold photoionization (Cell 2, 200 μ slits) of 50.0 mbar ($0.12 \times 10^{19} \text{ cm}^{-3}$) of CH_3I : a, 273K; b, 298K; c, 332K.

by Ivanov and Vilesov [8,9], we have subtracted an exponential background fitted to the zero baseline and the sharp photocurrent step at threshold. The resulting spectra, when analyzed for peak area (or peak height), yield plots identical in shape to those presented in Figs. 5 and 6.

Ivanov and Vilesov [8,9] discussed three bimolecular processes which, for a general dopant (D)/perturber (P) system, can be symbolized as



Eq. (3) represents electron attachment [16], while eq. (4) is associative ionization [16] (i.e., the Hornbeck-Molnar [12] process). Eq. (5) represents a photochemical rearrangement leading to charged species. In their discussion of pure CH_3I ($\text{D} = \text{P} = \text{CH}_3\text{I}$), Ivanov and Vilesov [8,9] discounted process (5) on the

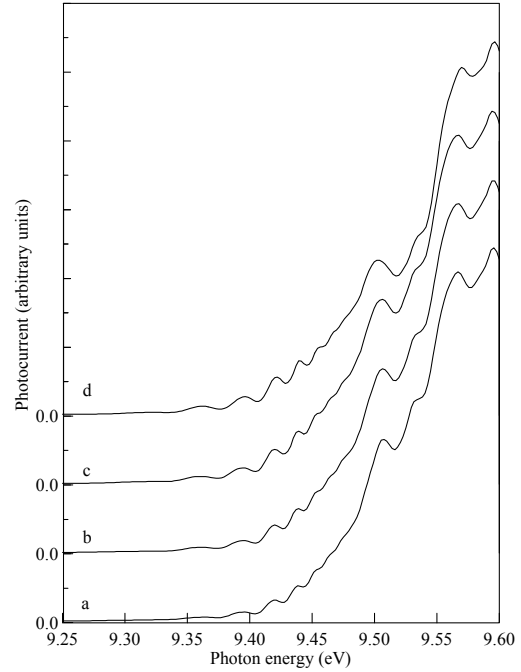


Fig. 4. Temperature dependence of subthreshold photoionization (Cell 1, 200 μ slits) of 1.0 mbar CH_3I in SF_6 ($0.14 \times 10^{19} \text{ cm}^{-3}$): a, 237K; b, 274K; c, 304K; d, 332K.

basis of energetic considerations.

If we assume that process (3) is saturated (i.e., independent of the perturber pressure) for a highly polarizable perturber, the electron attachment contribution to the photocurrent is given by

$$i_{ea} = k_1 \rho_D, \quad (6)$$

where the effective rate constant k_1 is proportional to the (saturated) electron attachment cross section, and we have assumed for the dopant number densities that $\rho_{D^*} \propto \rho_D$ in the linear absorption regime. Likewise, the associative ionization [process (4)] contribution to the photocurrent is given by

$$i_{ai} = k_2 \rho_D \rho_P, \quad (7)$$

where the effective rate constant k_2 is proportional to the associative ionization cross section, ρ_P is the perturber number density, and we have again assumed that $\rho_{D^*} \propto \rho_D$.

In the absence of any significant photochemical contribution [i.e., process (5)] to the

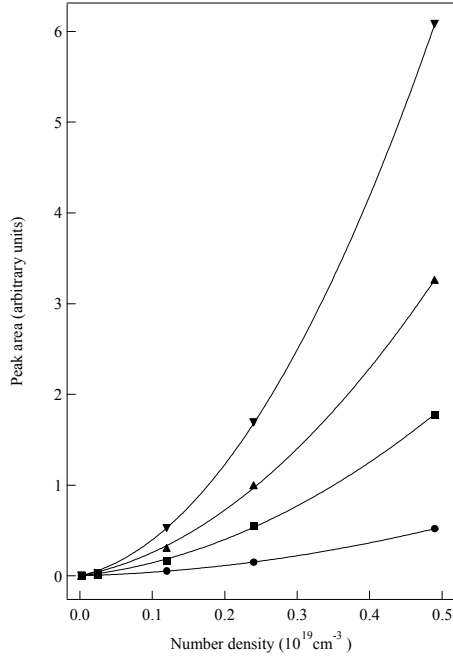


Fig. 5. Peak areas (by gaussian fits to the photoionization spectra) for the subthreshold photoionization structure (cf. Fig. 1) of pure CH_3I as a function of CH_3I number density ρ (10^{19} cm^{-3}). ●, 10d; ■, 11d; ▲, 12d; ▼, 13d. The solid lines represent a least-squares fit to the function $a_2 \rho^2 + a_1 \rho + a_0$ (cf. Table I).

observed signal, then, the subthreshold photocurrent should be given by

$$i = (k_1 + k_2 \rho_P) \rho_D, \quad (8)$$

Table I. Peak areas (by gaussian fits to the photoionization spectra) for the subthreshold photoionization structure (cf. Fig. 1) of pure CH_3I at varying number densities ρ (10^{19} cm^{-3}). The regression coefficients are for a least-squares second-order polynomial fit, $a_2 \rho^2 + a_1 \rho + a_0$, as shown in Fig. 5.

ρ	10d	11d	12d	13d
0.0024	0.00	0.00	0.00	0.00
0.025	0.00836	0.0128	0.0178	0.0254
0.12	0.0538	0.171	0.306	0.524
0.24	0.151	0.549	0.996	1.69
0.49	0.520	1.78	3.26	6.08

Regression Coefficients

a_0	0.00	0.00	0.00	0.00
a_1	0.229	0.863	1.41	1.99
a_2	1.73	5.63	10.9	21.1

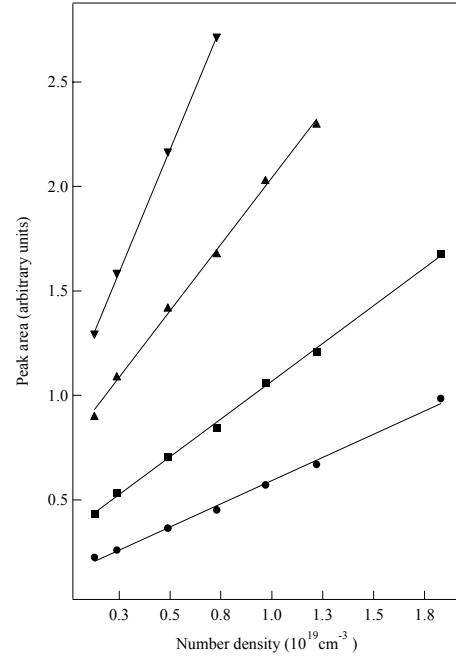


Fig. 6. Peak areas (by gaussian fits to the photoionization spectra) for the subthreshold photoionization structure (cf. Fig. 2) of 0.1 mbar CH_3I doped into SF_6 as a function of SF_6 number density ρ (10^{19} cm^{-3}). ●, 11d; ■, 12d; ▲, 13d; ▼, 14d. The solid lines represent a least-squares fit to the function $b_1 \rho + b_0$ (cf. Table II).

which accords with the data presented here for pure CH_3I ($\rho_P \equiv \rho_D \equiv \rho$) [cf. Fig. (5) and Table I],

$$i = a_1 \rho + a_2 \rho^2, \quad (9)$$

Table II. Peak areas (by gaussian fits to the photoionization spectra) for the subthreshold photoionization structure (cf. Fig. 2) of 0.1 mbar CH_3I in varying number densities ρ (10^{19} cm^{-3}) of SF_6 . The regression coefficients are for a least-squares linear fit, $b_1 \rho + b_0$, as shown in Fig. 6.

ρ	11d	12d	13d	14d
0.13	0.225	0.436	0.901	1.29
0.49	0.365	0.708	1.42	2.16
0.73	0.452	0.843	1.68	2.71
0.97	0.572	1.06	2.03	
1.22	0.670	1.21	2.30	

Regression Coefficients

b_0	0.101	0.376	0.690	0.990
b_1	0.444	0.768	1.40	2.39

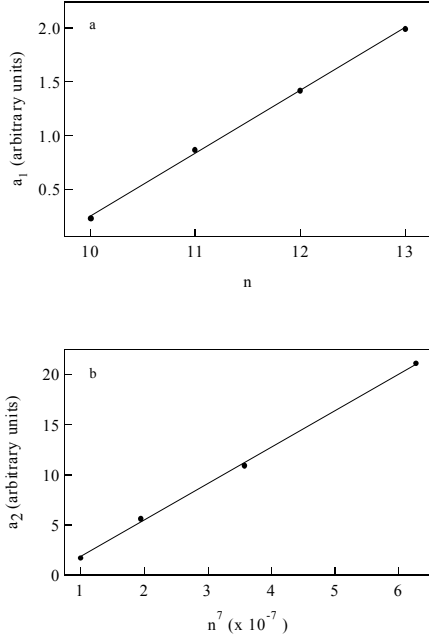


Fig. 7. (a) Linear and (b) quadratic regression coefficients for the subthreshold photoionization density dependence of pure CH_3I (Table I) plotted versus the CH_3I excited state principal quantum number n and n^7 , respectively. The straight lines are least-squares fits to the data. See text for discussion.

and for $\text{CH}_3\text{I}/\text{SF}_6$ ($\rho_p \equiv \rho$, $\rho_D = \text{constant}$) [cf. Fig. (6) and Table II],

$$i = b_0 + b_1 \rho. \quad (10)$$

From the analysis presented above, a_1 and b_0 should depend upon the dopant Rydberg electron attachment cross section in CH_3I and SF_6 , respectively. These cross sections scale linearly with the principal quantum number n for the CH_3I excited state [16]. A plot of a_1 vs n and b_0 vs n is presented in Fig. 7(a) and Fig. 8(a), respectively, and the linearity is indeed striking. Since a_2 and b_1 are reflective of a molecular interaction, these parameters should depend upon the excited state polarizability of CH_3I [17], which in turn scales according to n^7 [16]. A plot of a_2 vs n^7 and b_1 vs n^7 is presented in Fig. 7(b) and Fig. 8(b), respectively, and the linearity is again striking.

Clearly, the mechanisms of electron attachment and associative ionization are sufficient to explain the observed density

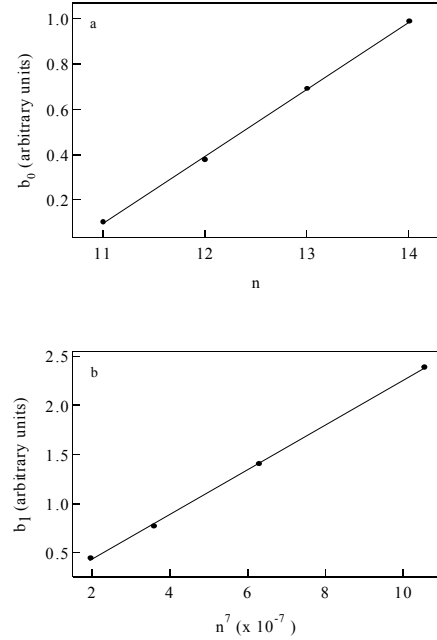


Fig. 8. (a) Constant and (b) linear regression coefficients for the subthreshold photoionization density dependence of $\text{CH}_3\text{I}/\text{SF}_6$ (Table II) plotted versus the CH_3I excited state principal quantum number n and n^7 , respectively. The straight lines are least-squares fits to the data. See text for discussion.

dependence of subthreshold photoionization. (A photochemical contribution [i.e., process (5)] is not positively ruled out, however, provided that such a mechanism scales as n (and is saturated) or as n^7 .)

The energy positions of a number of CH_3I and Rydberg states, as assigned from the photoionization spectra, for selected SF_6 number densities are given in Table III, as well as the values of I_1 extracted from a fit of the assigned spectra to the Rydberg equation. A plot of nd energies and I_1 as a function of SF_6 number density is shown in Fig. 9, where the red shift of all spectral features is readily apparent. Fig. 9 demonstrates that the peak positions depend linearly on the SF_6 number density, and that the resulting linear fits (obtained by regression analysis) are essentially parallel to one another.

The above result accords with the theory by Fermi [18], as modified by Alekseev and Sobel'man [19]. According to these authors [18,19], the total energy shift Δ is due to a sum

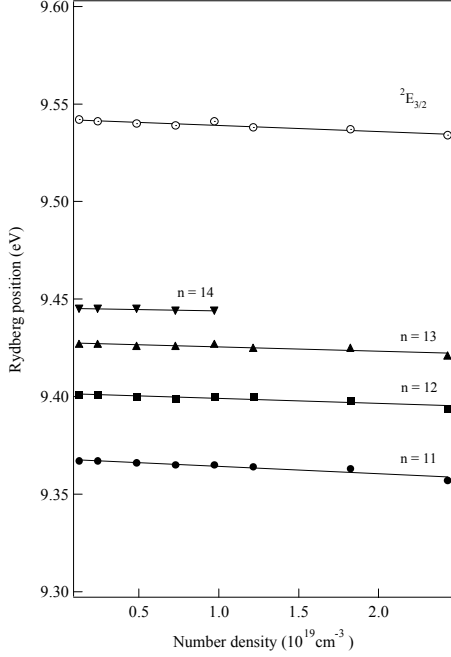


Fig. 9. Energy shifts of nd Rydberg states of CH_3I as a function of SF_6 number density ρ (10^{19} cm^{-3}). The fitted ionization energy I_1 is denoted ${}^2E_{3/2}$. All straight lines are least-squares fits.

of contributions

$$\Delta = \Delta_{\text{sc}} + \Delta_{\text{p}}, \quad (11)$$

where Δ_{sc} , the “scattering shift,” is due to the interaction of the Rydberg electron with the perturber molecule, while Δ_{p} , the “polarization shift,” results from the interaction of the positive core of the Rydberg molecule with the perturber molecule. Δ_{p} can be calculated from [2,13,19]

$$\Delta_{\text{p}} = -10.78 \left(\frac{1}{2} \alpha e^2 \right)^{2/3} (\hbar v)^{1/3} \rho. \quad (12)$$

In this equation, ρ is again the perturber number density, α the polarizability of the perturber molecule, e is the charge on the electron, \hbar is the reduced Planck constant, and v is the relative thermal velocity of the dopant and perturber molecules. Δ_{sc} results from a measurement of Δ , after calculating Δ_{p} .

Finally, the electron scattering length A of the perturber, which gauges the electron-perturber interaction, can easily be determined from [18]

TABLE III. nd and $I_1 \equiv I({}^2E_{3/2})$ photoionization energies (eV) of CH_3I in selected number densities ρ (10^{19} cm^{-3}) of SF_6 .

ρ	11d	12d	13d	14d	I_1
0.13	9.367	9.401	9.427	9.445	9.542
0.49	9.366	9.400	9.426	9.445	9.540
0.73	9.365	9.399	9.426	9.444	9.539
1.22	9.364	9.399	9.425		9.538
1.82	9.363	9.398	9.425		9.537
2.43	9.357	9.394	9.421		9.534

$$\Delta_{\text{sc}} = \left(\frac{2\pi\hbar^2}{m} \right) A \rho, \quad (13)$$

where m is the mass of the electron.

Since the slopes of the straight lines of Fig. 9 are essentially equal, one may assume that the average slope ($-25.14 \times 10^{-23} \text{ eV cm}^3$) closely approximates the asymptotic shift rate of the Rydberg series. Using the value [20] $\alpha = 6.54 \times 10^{-24} \text{ cm}^3$ for SF_6 , one finds from Eqs. (11-13) an electron scattering length for SF_6 of $A = -0.492 \text{ nm}$. This compares favorably to our recent measurement [13] of $A = -0.484 \text{ nm}$, from the analysis of autoionizing states in $\text{CH}_3\text{I}/\text{SF}_6$.

In summary, we have presented pressure-dependent and temperature-dependent subthreshold photoionization spectra of pure CH_3I and CH_3I doped into SF_6 . On the basis of these measurements, we were able to rule out vibrational autoionization as the mechanism of subthreshold ionization at high pressures, in contradistinction to the low-pressure case in pure CH_3I [9,11]. Moreover, we demonstrated a quadratic dependence on number density for the photocurrent signal in pure CH_3I , as reported previously [9], and a linear dependence on number density for the photocurrent signal in CH_3I doped into SF_6 . We then analyzed these dependences within a model that invoked both (saturated) electron attachment and associative ionization and found that the data presented are consistent with a Hornbeck-Molnar [12] mechanism leading to subthreshold photoionization in both cases. Nevertheless, only a mass analysis of photoproducts will

conclusively resolve this issue, as originally pointed out by Ivanov and Vilesov [9]. (This is particularly of interest in the case of SF₆, since this molecule weakly absorbs to a dissociative final state in this spectral region [21]. No photocurrent was detected in pure SF₆ in the energy region reported here, however.) Finally, we were able to evaluate the electron scattering length in SF₆ from the perturber density-dependent subthreshold photoionization data. The value presented is in accord with our previous measurement resulting from

autoionization studies in CH₃I/SF₆ [13].

ACKNOWLEDGMENT

This work was carried out at the University of Wisconsin Synchrotron Radiation Center (NSF DMR 95-31009) and was supported by grants from the National Science Foundation (CHE- 9506508) and from the Louisiana Board of Regents Support Fund (LEQSF (1997-00)-RD-A-14).

-
1. A. M. Köhler, R. Reininger, V. Saile and G. L. Findley, Phys. Rev. A **33**, 771 (1986).
 2. A. M. Köhler, R. Reininger, V. Saile and G. L. Findley, Phys. Rev. A **35**, 79 (1987).
 3. I. T. Steinberger, U. Asaf, G. Ascarelli, R. Reininger, G. Reisfeld and M. Reshotko, Phys. Rev. A **42**, 3135 (1990).
 4. U. Asaf, W. S. Felps, K. Rupnik and S. P. McGlynn, J. Chem. Phys. **91**, 5170 (1989).
 5. J. Meyer, R. Reininger, U. Asaf and I. T. Steinberger, J. Chem. Phys. **94**, 1820 (1991).
 6. U. Asaf, I. T. Steinberger, J. Meyer and R. Reininger, J. Chem. Phys. **95**, 4070 (1991).
 7. U. Asaf, J. Meyer, R. Reininger and I. T. Steinberger, J. Chem. Phys. **96**, 7885 (1992).
 8. V. S. Ivanov and F. I. Vilesov, Opt. Spectrosc. **36**, 602 (1974) [Opt. Spektrosk. **36**, 1023 (1974)].
 9. V. S. Ivanov and F. I. Vilesov, Opt. Spectrosc. **39**, 487 (1975) [Opt. Spektrosk. **39**, 857 (1975)].
 10. A. M. Köhler, Ph.D. thesis, Hamburg University, 1987 (unpublished).
 11. J. Meyer, U. Asaf and R. Reininger, Phys. Rev. A **96**, 1673 (1992).
 12. J. A. Hornbeck and J. P. Molnar, Phys. Rev. **84**, 621 (1951).
 13. C. M. Evans, R. Reininger and G. L. Findley, Chem. Phys. Letters, in press.
 14. A. K. Al-Omari and R. Reininger, J. Chem. Phys. **103**, 506 (1995).
 15. K. N. Altmann, A. K. Al-Omari and R. Reininger, Chem. Phys. Letters **261**, 597 (1996).
 16. T. F. Gallagher, *Rydberg Atoms* (Cambridge Univ. Press, Cambridge, 1994).
 17. J. O. Hirschfelder, C. F. Curtiss and R. B. Bird, *Molecular Theory of Gases and Liquids* (John Wiley, New York, 1964).
 18. E. Fermi, Nuovo Cimento **11**, 157 (1934).
 19. V. A. Alekseev and I. I. Sobel'man, Sov. Phys. JETP **22**, 882 (1966).
 20. R. D. Nelson and R. H. Cole, J. Chem. Phys. **54**, 4033 (1971).
 21. G. Herzberg, *Molecular Spectra and Molecular Structure. III. Electronic Spectra and Electronic Structure of Polyatomic Molecules* (Van Nostrand, New York, 1966).